Physica Scripta

PAPER

Studies of reflection asymmetry in heavy nuclei

P A Butler
Department of Physics, University of Liverpool, Liverpool L69 7ZE, United Kingdom
E-mail: peter.butler@liverpool.ac.uk

Keywords: nuclear structure, octupole collectivity, coulomb excitation

OPEN ACCESS

RECEIVED
22 November 2023

REVISED
11 January 2024

ACCEPTED FOR PUBLICATION
25 January 2024

PUBLISHED
8 February 2024

Abstract

For certain combinations of protons and neutrons it is expected that the shape of atomic nuclei can undergo octupole deformation, which would give rise to reflection asymmetry or a 'pear shape'. Here it is described how recent experiments carried out at CERN using the HIE-ISOLDE facility to accelerate radioactive beams and detect the subsequent γ-emission using the Miniball spectrometer have provided evidence that several radium and radon isotopes have either stable pear shapes or are octupole vibrational in nature. Their behaviour is compared with that of nuclei with $A \approx 150$ exhibiting strong octupole correlations. It will be shown that the data on transition moments present some challenges for theory. The relevance of these measurements for atomic EDM searches will also be discussed.

1. Introduction

It is well established by the observation of rotational bands that atomic nuclei can assume quadrupole deformation with axial and reflection symmetry, usually with the shape of a rugby ball. The distortion arises from long-range correlations between valence nucleons which becomes favourable when the proton and/or neutron shells are partially filled. For certain values of proton and neutron number it is expected that additional correlations will cause the nucleus to also assume an octupole shape (pear-shape) where it loses reflection symmetry in the intrinsic frame [1]. The observation of low-lying rotational bands with $K^{\pi} = 0^{-}$ in even–even nuclei is indicative of their having strong octupole correlations. Further evidence is provided by the sizeable value of the $E3$ moment for the transition to the ground state, indicating collective behaviour of the nucleons. However, the number of observed cases where the correlations are strong enough to induce a static pear-shape is much smaller. Strong evidence for this type of deformation comes from the observation of a particular behaviour of the energy levels for the rotating quantum system and from an enhancement in the E3 moment [2]. Prior to the present work experimental signatures in heavy nuclei have been observed for only two cases, ^{224}Ra [3] and ^{226}Ra [4]. This paper summarises new information on energy levels and electric matrix elements for the radioactive isotopes ^{222,224,226}Rn ($Z = 86$) and ^{222,228}Ra ($Z = 88$) obtained from recent experiments using the HIE-ISOLDE facility at CERN (for a brief review, see [5]). The behaviour of nuclei with $A \approx 220$ is compared here with that of isotopes with $Z \approx 58$, $A \approx 150$. Section 2.1 discusses how the experiments were performed, section 2.2 presents the new level-schemes for ^{224,226}Rn and compares the different rotational behaviour of nuclei with $A \approx 150$, $A \approx 220$, and sections 2.3 and 2.4 show the systematics of the electric transition matrix elements in both mass regions and a comparison of the experimental data with theory respectively. Section 3 discusses how nuclei with strong octupole correlations may be important for future searches that constrain the value of an electric dipole moment in atoms.

2. Experimental method and results

2.1. Coulomb excitation of radon and radium isotopes

The radioactive isotopes ^{224}Rn ($Z = 86$, $N = 138$) and ^{226}Rn ($Z = 86$, N = 140) ions were produced by spallation in a thick thorium carbide target bombarded by $\approx 10^{13}$ protons s^{-1} at 1.4 GeV from the CERN PS Booster [6, 7].

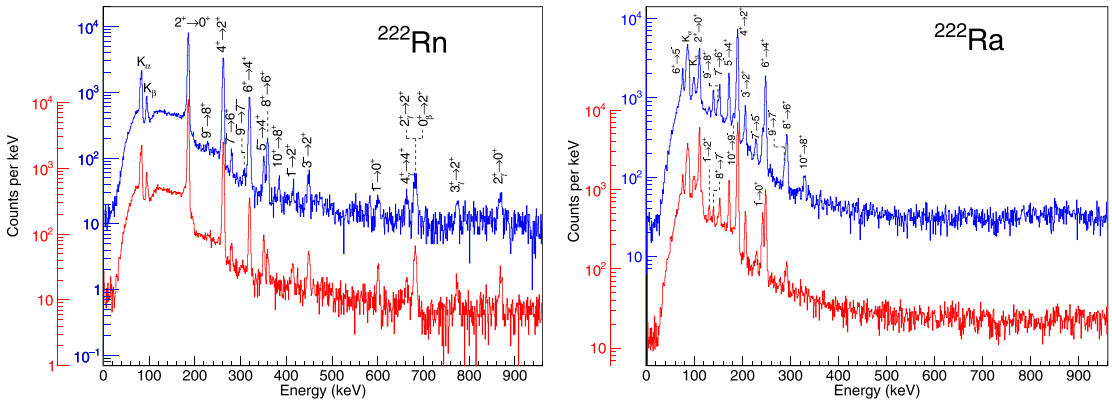

Figure 1. Spectra of γ rays emitted following the Coulomb excitation of ^{222}Rn and ^{222}Ra using a ^{120}Sn target (blue, upper), and ^{60}Ni (red, lower). The γ rays were corrected for Doppler shift assuming that they are emitted from the scattered projectile. Time-random coincidences between Miniball and the silicon detector have been subtracted. The transitions that give rise to the observed full-energy peaks are labelled by the spin and parity of the initial and final states. The spectra were obtained by sorting the data in the segment mode. Taken from [10, 11].

The reaction products diffused and effused from the heated target via a cooled transfer line towards an enhanced plasma ion source, which was used to singly ionize ($q = 1^+$) the Rn isotopes. The ions were accumulated and cooled in a Penning trap, REX-TRAP and delivered as a bunch to an electron-beam ion source, REX-EBIS at 500 ms intervals. Here, the charge-state of the ions was increased by charge breeding up to 51^+. The ions were accelerated in HIE-ISOLDE to an energy of 5.08MeV/u and bombarded secondary targets of 2.1 mg cm^{-2} ^{120}Sn. The post-accelerated beam intensities were 1.1×10^5 ions/s for ^{224}Rn and 2×10^3 ions/s for ^{226}Rn. The γ-rays emitted following the excitation of the target and projectile nuclei were detected in Miniball [8], an array of 24 high-purity germanium detectors, each with six-fold segmentation and arranged in eight triple-clusters. For the γ-γ measurements described in section 2.2 the recorded energies were taken from the core of each crystal and events were rejected when hits were recorded in the adjacent crystals within the triple-cluster, in order to reduce the background from Compton scattering. For all the experiments described here the scattered projectiles and target recoils were detected in a highly segmented silicon detector [9].

In addition, ^{222}Ra ($Z = 88, N = 134$) and ^{228}Ra (Z=88, $N = 140$) were produced by spallation in a thick uranium carbide primary target again bombarded by $\approx 10^{13}$ protons s^{-1} at 1.4 GeV [10]. The ions, extracted from a tungsten surface ion source were stripped to charge states of 51^+ and 53^+, respectively, for ^{222}Ra and ^{228}Ra and accelerated in HIE-ISOLDE to an energy of 4.31MeV/u. The radioactive beams, with intensities between 5×10^4 and 2×10^5 ions/s bombarded secondary targets of ^{60}Ni and ^{120}Sn of thickness 2.1 mg cm^{-2}. Gamma rays and scattered ions emitted following the excitation of the target and projectile nuclei were detected as before. Also, ^{222}Rn ($Z = 86, N = 136$) ions were produced in the same manner as for ^{224,226}Rn and accelerated in HIE-ISOLDE to 4.23 MeV/u [11]. The accelerated ions then bombarded, with an intensity of 6×10^5 ions/s, the ^{60}Ni and ^{120}Sn targets as before. The aim of these experiments was to measure electromagnetic matrix elements in ^{222}Rn, ^{222}Ra and ^{228}Ra, see section 2.3. The distance of closest approach $\geqslant R_1 + R_2 + 5$ fm, where R_1, R_2 are the beam, target nuclear radii, ensuring that the contribution from nuclear interactions is negligible [12]. The recorded γ-ray energies were taken from either the core of each Miniball crystal (for the ^{222}Rn measurements) or from each of the six individual segments of the crystal (for ^{222}Rn, ^{222,228}Ra). In the latter mode the Compton background was reduced by rejecting events if a second hit was recorded in another segment in the same crystal. Use of this detector configuration improved the quality of the spectra in the cases where the instantaneous count rate was high.

Representative γ-ray spectra obtained for ^{222}Rn and ^{222}Ra from both the ^{120}Sn and ^{60}Ni targets are presented in figure 1. As the cross section for the Coulomb excitation of the projectile is strongly dependent on the atomic number of the target, the use of two targets with significantly different values of Z produce a different population of states in the heavy radon and radium nuclei. In particular, the higher-Z target ^{120}Sn allows access to higher-spin states through multistep Coulomb excitation compared with ^{60}Ni. The spectra reveal a strong population of the positive-parity states of the ground-state band, which are populated via multiple $E2$ excitation. In nuclei that are unstable to pear-shaped distortion, the other favoured excitation paths are to members of the octupole band, in which the negative-parity states are coupled to the ground-state band by strong $E3$ transitions. These states will decay to states in the ground-state band by fast $E1$ transitions. What is evident in the figure is the significantly stronger population of both positive- and negative-parity states in ^{222}Ra compared to those in ^{222}Rn, arising from the larger intrinsic quadrupole and octupole moments in the radium isotopes compared to radon, see

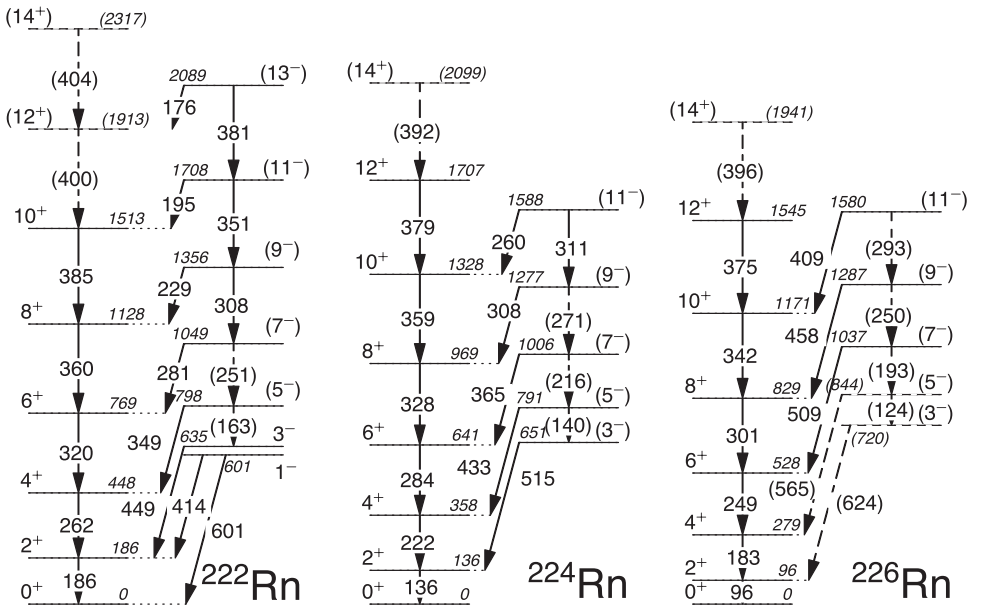

Figure 2. Rn level schemes. These partial level-schemes for ^{222,224,226}Rn show the excited states of interest. Arrows indicate γ-ray transitions. All energies are in keV. Firm placements of transitions in the scheme are from previous work [15] or have been made using $\gamma-\gamma$-ray coincidence relations [6, 7]. The spin and parity assignments for the positive-parity band that is strongly populated by Coulomb excitation can be regarded as firm, whereas the negative-parity state assignments are made in accord with the systematic behaviour of nuclei in this mass region.

sub-section 2.3. Also of interest is the presence of low-lying collective bands labelled β (built on an excited $K^\pi = 0^+$ band-head) and γ (built on an excited $K^\pi = 2^+$ band-head) observed for the first time in ^{222}Rn. Their placement in the level scheme was determined through analysis of a $\gamma-\gamma$ coincidence matrix collected with data from both targets. The feeding from the so-called β-band to the negative-parity states is appreciable (see figure 8 in [11]) and has to be taken into account in the determination of $E3$ matrix elements (section 2.3). Low-lying collective bands are also observed in the Coulomb excitation of ^{220}Rn [3], ^{224}Ra [3] and ^{228}Ra [10] but are populated very weakly in the case of ^{222}Ra, see figure 1. Strong excitation of the β-band with enhancement of the $E3$ coupling to the negative-parity band is also observed in ^{148}Nd, for which it is suggested that there is a significant component of the two-phonon octupole vibration in the wavefunction of the β-band [13]. More recently low-lying 0_2^+ levels have been described as 2p-2h exctations (see [14] and references therein) which can easily couple strongly to both the ground-state and octupole band.

2.2. Characterisation of octupole instability from rotational behaviour

Prior to the experiments discussed here, nothing was known about the energies and spins of excited states in ^{224,226}Rn, while de-exciting γ-rays from states in ^{222}Rn had been observed [15] up to $I^\pi = 13^-$. In order to determine the decay scheme of ^{224,226}Rn, pairs of coincident γ-rays were examined. In this analysis, the energy spectrum of γ-rays coincident with one particular transition is generated by requiring that the energy of this gating transition lies in a specific range. In this way the level schemes for ^{224,226}Rn could be constructed from the coincidence spectra [6, 7]. These schemes, together with the known [15] scheme for ^{222}Rn, are shown in figure 2.

The character of the octupole bands can be explored [15] by examining the difference in aligned angular momentum, $\Delta i_x = i_x^- - i_x^+$, at the same rotational frequency ω as a function of ω, as shown in figures 3 and 4. Here i_x is approximately I for $K = 0$ bands and $\hbar\omega$ is approximately $(E_I - E_{(I-2)})/2$. For octupole vibrational nuclei in which the negative-parity states arise from coupling an octupole phonon to the positive-parity states, it is expected that $\Delta i_x \approx 3\hbar$ as the phonon prefers to align with the rotational axis [16]. This appears to be the case for nuclei with $Z \approx 56$, $N \approx 88$ at values of $\hbar\omega < 0.2$ MeV where particle-hole excitations do not play a role, see figure 3. Above this rotational frequency there is some evidence that reflection-asymmetric and reflection-symmetric shapes can co-exist in nuclei. Urban *et al* have observed a crossing of the positive-parity sequence of the octupole band in ^{150}Sm with a band corresponding to a reflection symmetric shape, possibly related to a rotational alignment in the ground-state band at $\hbar\omega \approx 0.3$ MeV [17]. After the crossing reflection symmetric and asymmetric nuclear shapes are considered to coexist. In another example, the ground-state octupole band in ^{222}Th is not seen beyond spin $25\hbar$ ($\hbar\omega \approx 0.25$ MeV) in contrast to ^{220}Ra where the highest spin seen is 31 $\hbar$ [18]. These observations are consistent with Woods-Saxon-Bogolyubov cranking calculations which predict that the ground-state band in ^{222}Th will cross a reflection-symmetric four-quasiparticle band at $I = 24\hbar$, whereas the

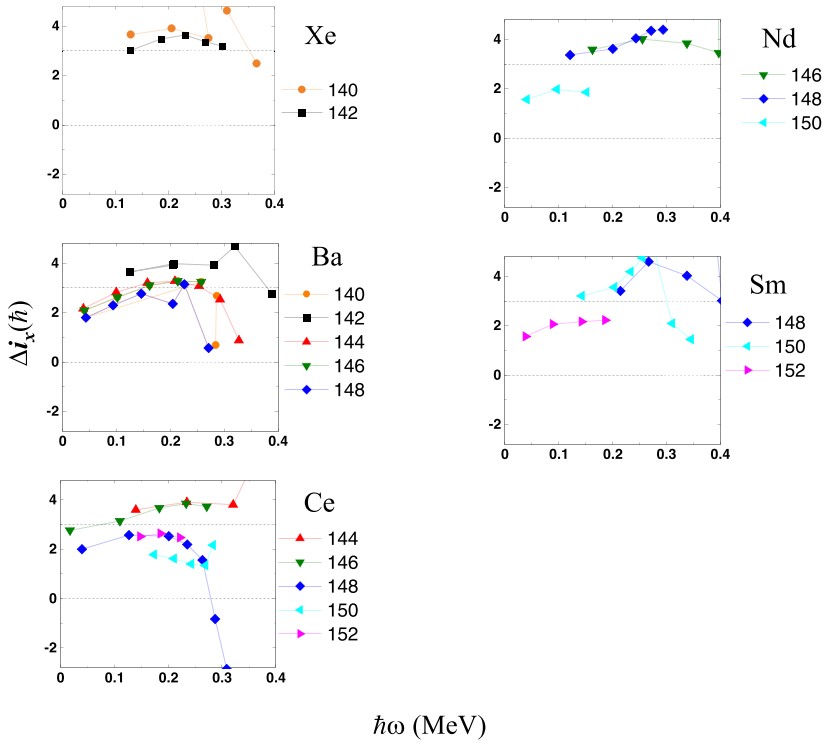

Figure 3. Systematic rotational behaviour of Xe, Ba, Ce, Nd, and Sm isotopes, showing the difference in aligned spin for negative- and positive-parity states as a function of rotational frequency. The dashed line at $\Delta i_x = 0$ is the expected value for static octupole deformation, the line at $\Delta i_x = 3\hbar$ corresponds to octupole vibration. Taken from [21].

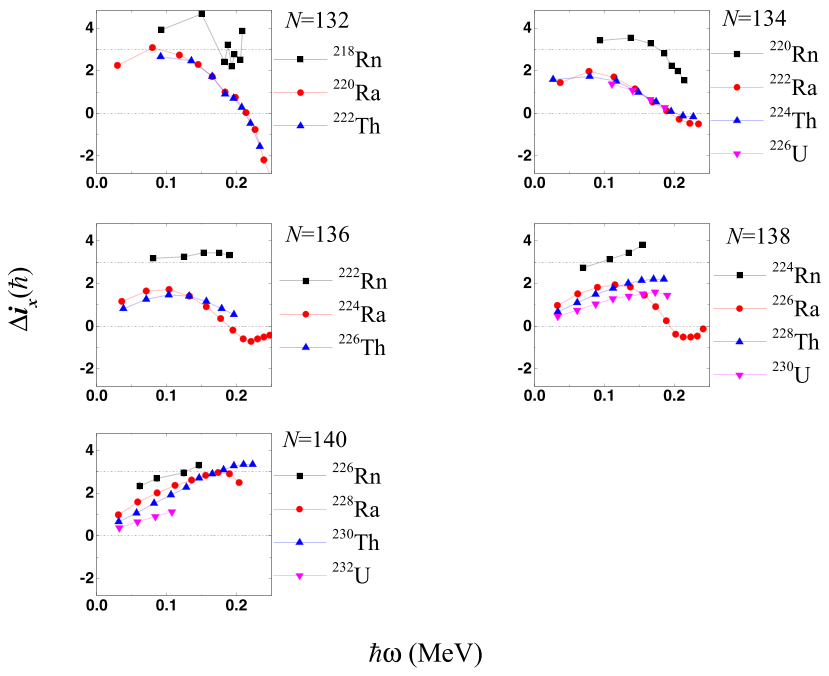

Figure 4. Systematic rotational behaviour of Rn, Ra, Th, and U isotopes, showing the difference in aligned spin for negative- and positive-parity states as a function of rotational frequency. The dashed line at $\Delta i_x = 0$ is the expected value for static octupole deformation, the line at $\Delta i_x = 3\hbar$ corresponds to octupole vibration. Taken from [21].

yrast band in ^{220}Ra is predicted to maintain its reflection asymmetry to higher spins [19]. In contrast, $^{238-240}$Pu, which have octupole-vibrational behaviour at low spin, are found to exhibit properties associated with stable octupole deformation at the highest spins, suggesting that a transition from a vibration to stable deformation may have occurred [20].

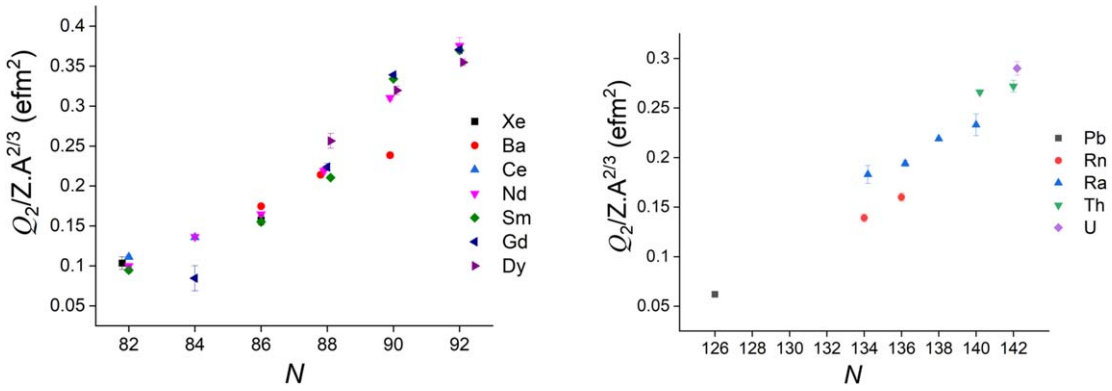

Figure 5. The systematics of measured $E2$ intrinsic moments Q_2 for $0^+ \rightarrow 2^+$ transitions for medium-mass nuclei with $Z \geqslant 50$, $N \geqslant 82$ and heavy nuclei with $Z \geqslant 82$, $N \geqslant 126$. For the source of the data shown here, see [48], figure 4 in [21], and [11].

Octupole-vibrational behaviour is also observed for all the radon isotopes and Ra, Th and U isotopes with $N = 140$, see figure 4. For nuclei with permanent octupole deformation Δi_x is expected to approach zero, as observed for several isotopes of Ra, Th, and U [21], see figure 4. Here, deviations are seen at low rotational frequencies because the negative-parity band is displaced relative to the positive-parity band near the ground state. This displacement is associated with the lowering of the barrier at $\beta_3 = 0$ between the reflection-asymmetric shapes, which is a consequence of pairing at low spin for even–even nuclei [22, 23]. It should be noted that this rotational behaviour can also be interpreted as the condensation of rotational-aligned octupole phonons in which the nucleus assumes a heart shape for $N \approx 136$ [24].

2.3. Measurement of $E\lambda$ matrix elements in radon and radium isotopes

Values of $E1$, $E2$ and $E3$ matrix elements in ^{222}Rn [11], ^{222}Ra [10] and ^{228}Ra [10] were obtained by using the Coulomb-excitation least-squares fitting code GOSIA [25]. GOSIA was employed to calculate excitation probabilities and subsequent γ-ray decay intensities of excited states for a given set of electromagnetic matrix elements. The calculated γ-ray intensities can be compared with the experimental yields and additional spectroscopic information that is available. In this work, known γ-ray branching ratios of low lying negative-parity states together with the measured γ-ray intensities were included in the calculations. A standard χ^2 function for both yields and branching ratios was constructed which was minimized by varying the values of the electromagnetic matrix elements between all relevant states, treated as free parameters. For all three nuclei the excitation and decay of low-lying β and γ collective bands were also taken into account in the GOSIA fit; as remarked in section 2.1 the decay of the β-band to the negative-parity states in particular influences the fitted values of the $E3$ matrix elements connecting the octupole and ground-state bands. In order to determine the systematic sources of errors, a number of independent fits was obtained with different initial conditions. These included varying the target thickness, the beam energy, the distance between the target and the particle detector, the efficiency of the Miniball detectors, the $E4$ matrix elements, and the signs of the $E2$ couplings to the higher-lying collective bands.

The measured values of normalised quadrupole moment $Q_2/Z.A^{2/3}$ for nuclei with $Z \geqslant 50$, $N \geqslant 82$ and $Z \geqslant 82$, $N \geqslant 126$ are shown in figure 5. This quantity, proportional to the quadrupole deformation parameter β_2, shows a steady increase with N as it approaches the mid-shell value. In contrast the normalised octupole moment $Q_3/Z.A$, proportional to the octupole deformation parameter β_3, stays approximately constant with N, see figure 6. In these figures the intrinsic moments Q_λ are derived from the transition matrix elements $\langle I_i||\mathcal{M}(E\lambda)||I_f\rangle$ assuming the validity of the rotational model. The value of Q_2 was derived from $\langle 0^+||\mathcal{M}(E2)||2^+\rangle$ or $\langle 2^+||\mathcal{M}(E2)||4^+\rangle$; Q_3 was derived from the matrix element corresponding to the $0^+ \rightarrow 3^-$ transition except for Rn, Ra where Q_3 is averaged over several transitions. For $82 \leqslant N \leqslant 88$, there is no observed enhancement for Q_3 within experimental uncertainties, while for $N > 88$ the $E3$ strength is no longer concentrated in the lowest octupole band but is shared among this band and bands with other modes of octupole shape oscillations that occur in deformed nuclei. These other modes will come down in energy as the number of protons and neutrons move away from the closed shell at $Z = 50$, $N = 82$ (or at $Z = 82$, $N = 126$). In contrast, the larger values of Q_3 for ^{222}Ra, ^{224}Ra and ^{226}Ra indicate an enhancement in octupole collectivity that is consistent with an onset of octupole deformation in this mass region.

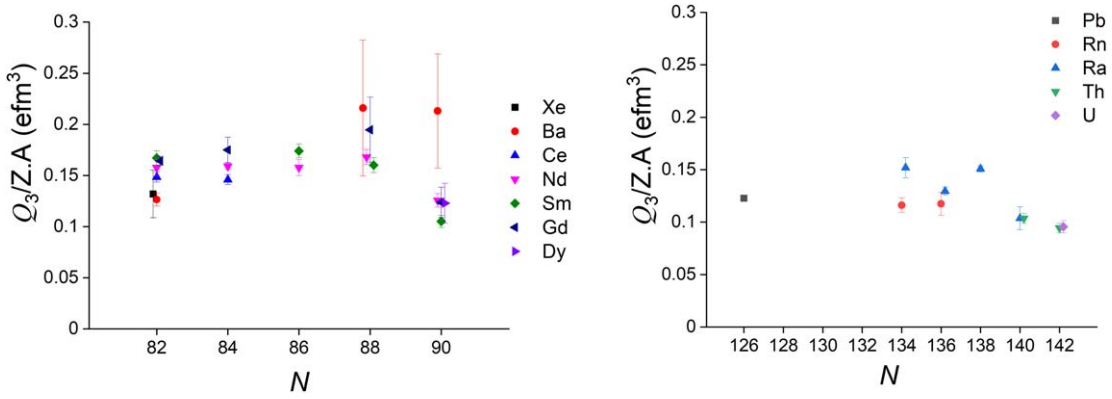

Figure 6. The systematics of measured $E3$ intrinsic moments Q_3 for medium-mass nuclei with $Z \geqslant 50$, $N \geqslant 82$ and heavy nuclei with $Z \geqslant 82$, $N \geqslant 126$. The values of Q_λ are calculated for the $0^+ \rightarrow 2^+$ or $0^+ \rightarrow 3^-$ transitions except for the values of Q_3 for the isotopes of Rn, Ra. For these isotopes the uncertainty in Q_3 is reduced by evaluating a weighted average of Q_3 for several $I \rightarrow I + 3$ transitions where it has been measured. For the source of the data shown here, see figures 4, 5 in [21], and [11].

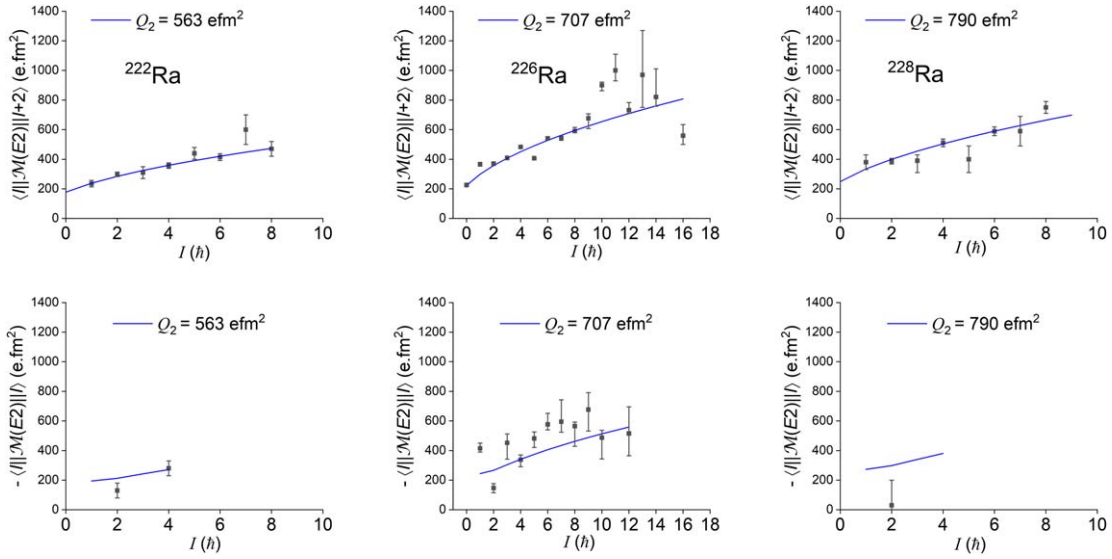

Figure 7. Values of the $E2$ matrix elements for various transitions in ^{222,226,228}Ra isotopes. The line through the data is the fitted value assuming a constant value of Q_2 and the validity of the rotational model. The data are taken from [4, 10].

2.4. Comparison of experimental $E\lambda$ matrix elements with theory

The values of $\langle I_i||\mathcal{M}(E\lambda)||I_f\rangle$ for $E2$ transitions and for $E3$ transitions in ^{222,226,228}Ra are shown in figures 7 and 8 respectively as a function of spin. In each of the figures, a smooth line that is fitted to the matrix elements assuming a constant Q_λ is also shown. It is observed that the values of Q_2 for the transitions in ^{222,226,228}Ra and Q_3 for the transitions in ^{222,226}Ra are approximately constant, consistent with the picture of a rotating pear shape for the lighter radium isotopes. In contrast, the values of $\langle 2^+||\mathcal{M}(E3)||3^-\rangle$ and $\langle 1^-||\mathcal{M}(E3)||4^+\rangle$ in ^{228}Ra do not show the same behaviour. Staggering in the values of Q_λ with spin have been predicted using the Gogny Hartree–Fock-Bogoliubov + interacting boson model [26] but these do not reproduce the observations for either the Q_2 or Q_3 moments. The values of $\langle 2^+||\mathcal{M}(E3)||3^-\rangle$ and $\langle 1^-||\mathcal{M}(E3)||4^+\rangle$ are also observed to be anomalously low in ^{148}Nd and ^{150}Nd, see figure 12 in [2]. Their behaviour in ^{148}Nd can be reproduced approximately using a quadrupole-octupole coupling model [13].

The experimental values of intrinsic dipole and octupole moments Q_1 and Q_3 for radium isotopes, corresponding to the $0^+ \rightarrow 1^-$ ($E1$) and $0^+ \rightarrow 3^-$ ($E3$) transitions, are compared with various theoretical calculations in figure 9. The calculations are from macroscopic-microscope (MaMi) [27, 28], relativistic mean field (NLSH) [29], cranked Skyrme-Hartree–Fock (SkIII) [30], Skyrme-Hartree–Fock (SkO′) [31], cluster model (Clus) [32], Gogny Hartree–Fock-Bogoliubov (D1M2d) [33], quadrupole-octupole collective Hamiltonian based on the PC-PK1 relativistic density functional (QOCH, QOCH′) [34, 35], Skyrme Hartree–Fock-Bogoliubov (UNEDF0) [36] and Gogny Hartree–Fock-Bogoliubov + interacting boson model (D1MIBM) [26]

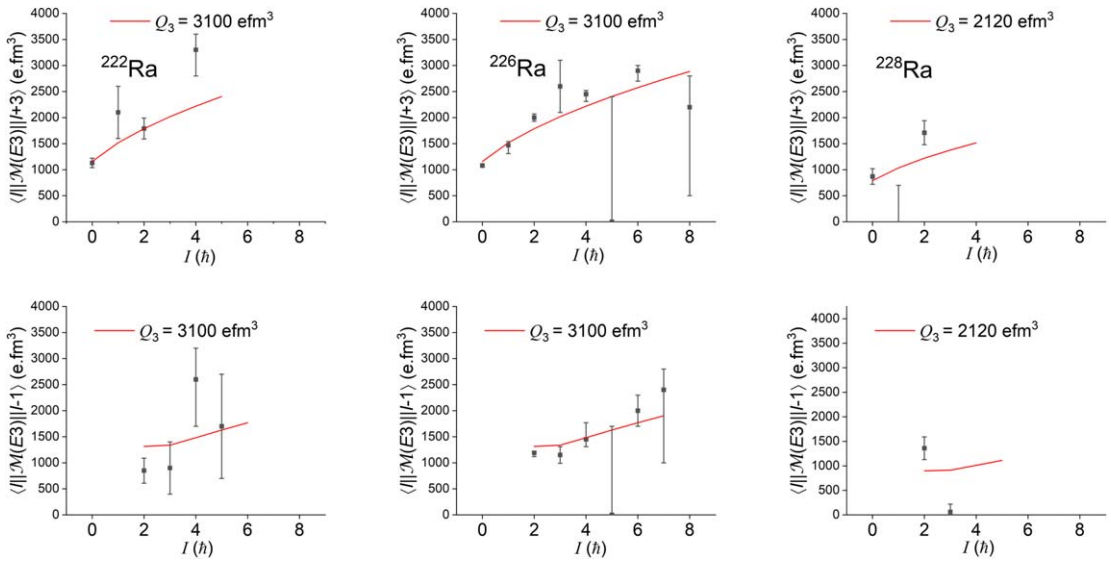

Figure 8. Values of the $E3$ matrix elements for various transitions in ^{222,226,228}Ra isotopes. The line through the data is the fitted value assuming a constant value of Q_3 and the validity of the rotational model. The data are taken from [4, 10].

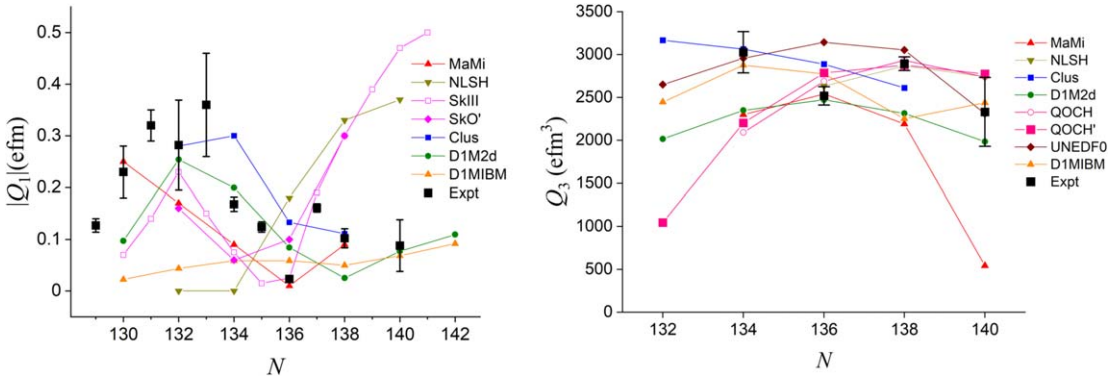

Figure 9. Measured values (Expt) of intrinsic octupole moments, Q_1 for $0^+ \rightarrow 1^-$ (left), and Q_3 for $0^+ \rightarrow 3^-$ (right) transitions as a function of N for radium isotopes, compared with values calculated using various theoretical models. For details of the calculations see the text.

calculations. For the behaviour of Q_1 with neutron number, only the microscopic theories are able to exhibit a minimum around $N = 134 - 138$; not all of these are able to reproduce the observed minimum for ^{224}Ra. In contrast, there is good agreement between the various calculations and the experimental values of Q_2 (see figure 17 in [2]). On the other hand a wide variation in the predicted values of Q_3 from the different theories is evident, although no particular model description can be favoured or discarded on the basis of the experimental data. The systematic behaviour of energy levels in certain isotopes of thorium and uranium nuclei suggests that these may also be pear shaped, see figure 4. Several calculations using Gogny Hartree–Fock-Bogoliubov (D1M) [37], quadrupole-octupole collective Hamiltonian based on the PC-PK1 relativistic density functional (QOCH′) [38] and Gogny Hartree–Fock-Bogoliubov + interacting boson model (D1MIBM′) [39] predict very large values of E3 moments in thorium and uranium isotopes with $N \approx 136 - 138$ (see figure 10). Experiments to measure $E3$ transition probabilities in these heavier nuclei await advances in radioactive beam technology that should be realized in the next few years.

3. Reflection-asymmetric shapes and atomic electric-dipole moments

The fact that some nuclei can have a reflection-asymmetric shape has influenced the choice of atoms having odd-A nuclei employed to search for permanent electric-dipole moments (EDMs). Any measurable moment will be amplified if the nucleus has octupole collectivity and further enhanced by static-octupole deformation. At present, experimental limits on EDMs, that would indicate charge-parity (CP) violation in fundamental

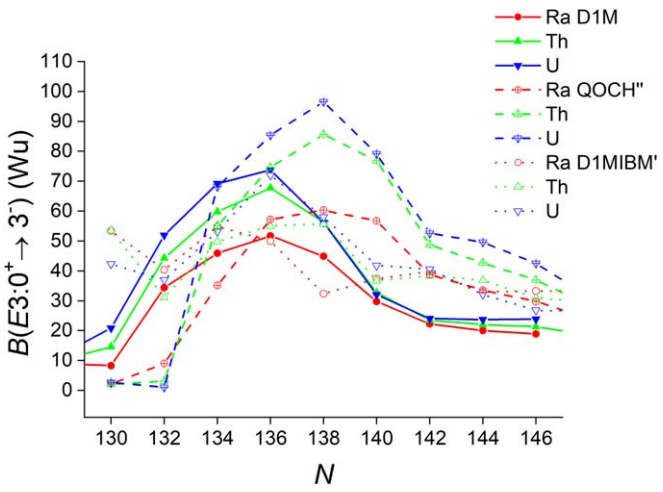

Figure 10. Theoretical values of $B(E3\colon 0^{+} \rightarrow 3^{-})$ transition strengths (in single particle units) versus N for various isotopes of Ra, Th and U. For details of the calculations see the text.

processes where flavour is unchanged, have placed severe constraints on many extensions of the Standard Model. For certain isotopes octupole effects are expected to enhance, by a factor 100–1000, the nuclear Schiff moment (the electric-dipole distribution weighted by radius squared) that induces the atomic EDM [40–43], thus improving the sensitivity of the measurement. There are two factors that contribute to the greater electrical polarizability that causes the enhancement: (i) the odd-A nucleus assumes an octupole shape; (ii) an excited state lies close in energy to the ground state with the same angular momentum and intrinsic structure but opposite parity. Such parity doublets arise naturally if the deformation is static (permanent octupole deformation). Candidate atomic species with nuclei having strong octupole correlations, such as ^{221}Rn, ^{225}Ra, ^{229}Pa, have been proposed for EDM searches [44, 45]. The measurements described here lead to the conclusion that the even–even nuclei $^{222-226}$Ra have octupole-deformed character, and their odd-mass neighbours ^{223,225}Ra, having parity doublets separated by ≈50 keV, should have large enhancement of their Schiff moments. Measurements of the *E*3 strength in odd-*A* nuclei have yet to be carried out, however. For the octupole-vibrational radon isotopes, it appears unlikely that odd-*A* nuclei such as ^{221,223,225}Rn will have low-lying parity doublets. Bands of opposite parity with differing single-particle configurations can lie close to each other fortuitously but in general those arising from coupling the odd nucleon to the ground state and octupole phonon will be well separated. The separation will be determined by the spacing of the bands in the even–even core, ≈500 keV in the case of $^{222-226}$Rn, and any enhancement of the Schiff moment will be smaller in radon atoms than for radium atoms. In the case of ^{229}Pa evidence was presented many years ago [46] for the occurrence of a 5/2 parity doublet with splitting of ≈200 eV. If this were the case then there would be considerable enhancement of the nuclear Schiff moment, making ^{229}Pa the best candidate for atomic EDM searches. However, the same authors have more recently cast doubt on the existence of this doublet [47], and have proposed new measurements that could resolve this issue.

4. Summary

There is now a substantial body of evidence, from the behaviour of the energies of quantum states and the interconnecting electromagnetic matrix elements, particularly electric octupole matrix elements, that a few isotopes of radium have permanent octupole deformation, i.e. are pear shaped. This is important not just for testing nuclear theories but also for improving the sensitivity of atomic EDM searches that could reveal the violation of fundamental symmetries not accounted for by the standard model.

Acknowledgments

I am grateful to Niels Bidault, Eleftherios Fadakis, Karl Johnston, Miguel Lozano, Jose Alberto Rodriguez, Sebastian Rothe, Erwin Siesling, and Fredrick Wenander who assisted with the preparation of the radioactive beams, and Liam Gaffney, Pietro Spagnoletti, Joonas Konki, Marcus Scheck, John Smith, Kenzo Abrahams, Michael Bowry, Joakim Cederkäll, Timothy Chupp, Giacomo de Angelis, Hilde De Witte, Paul Garrett, Alina Goldkuhle, Corinna Henrich, Andres Illana, David Joss, James Keatings, Nicola Kelly, Michalina Komorowska,

Thorsten Kröll, Bondili Nara Singh, David O'Donnell, Joonas Ojala, Robert Page, Line Pedersen, Christopher Raison, Peter Reiter, Dawid Rosiak, Timur Shneidman, Burkhard Siebeck, Michael Seidlitz, Jacqueline Sinclair, Marek Stryjczyk, Piet Van Duppen, Silvia Vinals, Ville Virtanen, Nigel Warr, Kasia Wrzosek-Lipska and Magda Zielińska who assisted with the data collection and analysis. The support of the ISOLDE Collaboration and technical teams is also acknowledged. I also thank Kosuke Nomura, Zhipan Li and Shuangquan Zhang for providing me with the results of their calculations. This work was supported by the following Research Councils and Grants: Science and Technology Facilities Council (UK) Grants No. ST/P004598/1, No. ST/L005808/1, No. ST/R004056/1; Federal Ministry of Education and Research (Germany) Grants No. 05P18RDCIA, No. 05P15PKCIA, and No. 05P18PKCIA and the 'Verbundprojekt 05P2018'; National Science Centre (Poland) Grant No. 2015/18/M/ST2/00523; European Union's Horizon 2020 Framework research and innovation programme 654 002 (ENSAR2); Marie Skłodowska-Curie COFUND Grant (EU-CERN) 665 779; Research Foundation Flanders and IAP Belgian Science Policy Office BriX network P7/12 (Belgium); GOA/2015/010 (BOF KU Leuven); RFBR (Russia) Grant No. 17-52-12015; the Academy of Finland (Finland) Grant No. 307 685; the Bulgarian National Science Fund (BNSF) under Contract No. KP-06-N48/1.

Data availability statement

All data that support the findings of this study are included within the article (and any supplementary files).

ORCID iDs

P A Butler https://orcid.org/0000-0001-6080-9205

References

[1] Butler P A and Nazarewicz W 1996 *Rev. Mod. Phys.* **68** 349–421
[2] Butler P A 2016 *J. Phys. G: Nucl. Part. Phys.* **43** 073002
[3] Gaffney L P *et al* 2013 *Nature* **497** 199–204
[4] Wollersheim H J *et al* 1993 *Nucl. Phys.* A **556** 261–80
[5] Butler P A 2023 *J. Phys.: Conf. Ser.* **2453** 012001
[6] Butler P A *et al* 2019 *Nat. Commun.* **10** 2473
[7] Butler P A *et al* 2020 *Nat. Commun.* **11** 3560
[8] Warr N *et al* 2013 *Eur. Phys. J.* A **49** 40
[9] Ostrowski A N, Cherubini S, Davinson T, Groombridge D, Laird A M, Musumarra A, Ninane A, di Pietro A, Shotter A C and Woods P J 2002 *Nucl. Instrum. Methods* A **480** 448–55
[10] Butler P A *et al* 2020 *Phys. Rev. Lett.* **124** 042503
[11] Spagnoletti P *et al* 2022 *Phys. Rev.* C **105** 024323
[12] Cline D 1986 *Annu. Rev. Nucl. Part. Sci.* **36** 683–716
[13] Ibbotson R W *et al* 1997 *Nucl. Phys.* A **619** 213–40
[14] Sharpey-Schafer J F 2023 *Eur. Phys. J.* A **59** 183
[15] Cocks J F C *et al* 1999 *Nucl. Phys.* A **645** 61–91
[16] Rohoziński S G 1988 *Rep. Prog. Phys.* **51** 541–603
[17] Urban W, Lieder R M, Gast W, Hebbinghaus G, Kramer-Flecken A, Blume K P and Hübel H 1987 *Phys. Lett.* B **185** 331–5
[18] Smith J F *et al* 1995 *Phys. Rev. Lett.* **75** 1050–3
[19] Nazarewicz W, Leander G A and Dudek J 1987 *Nucl. Phys.* A **467** 437–60
[20] Wiedenhöver I *et al* 1999 *Phys. Rev. Lett.* **83** 2143–6
[21] Butler P A 2020 *Proc. R. Soc. London* A **476** 2020020
[22] Brink D M, Buck B, Huby R, Nagarajan M A and Rowley N 1987 *J. Phys. G: Nucl. Phys.* **13** 629–49
[23] Egido J L and Robledo L M 1989 *Nucl. Phys.* A **494** 85–101
[24] Frauendorf S 2008 *Phys. Rev.* C **77** 021304(R)
[25] Zielińska M, Gaffney L P, Wrzosek-Lipska K, Clément E, Grahn T, Kesteloot N, Napiorkowski P, Pakarinen J, Van Duppen P and Warr N 2016 *Eur. Phys. J.* A **52** 99
[26] Nomura K, Rodríguez-Guzmá R, Humadi Y M, Robledo L M and García-Ramos J E 2020 *Phys. Rev.* C **102** 064326
[27] Nazarewicz W, Olanders P, Ragnarsson I, Dudek J, Leander G A, Möller P and Ruchowska E 1984 *Nucl. Phys.* A **429** 269–95
[28] Butler P A and Nazarewicz W 1991 *Nucl. Phys.* A **533** 249–68
[29] Rutz K, Maruhn J A, Reinhard P-G and Greiner W 1995 *Nucl. Phys.* A **590** 680–702
[30] Tsvetkov A, Kvasil J and Nazmitdinov R G 2002 *J. Phys. G: Nucl. Part. Phys.* **28** 2187–206
[31] Engel J, Bender M, Dobaczewski J, de Jesus J H and Olbratowski P 2003 *Phys. Rev.* C **68** 025501
[32] Shneidman T M, Adamian G G, Antonenko N V, Jolos R V and Scheid W 2003 *Phys. Rev.* C **67** 014313
[33] Robledo L M and Butler P A 2013 *Phys. Rev.* C **88** 051302(R)
[34] Sun W, Quan S, Li Z P, Zhao J, Nikšić T and Vretenar D 2019 *Phys. Rev.* C **100** 044319
[35] Zhang W and Zhang S Q 2019 *Phys. Rev.* C **100** 054303
[36] Cao Y, Agbemava S E, Afanasjev A V, Nazarewicz W and Olsen E 2020 *Phys. Rev.* C **102** 024311
[37] Robledo L M and Bertsch G F 2011 *Phys. Rev.* C **84** 054302
[38] Xia S Y, Tao H, Lu Y, Li Z P, Nikšić T and Vretenar D 2017 *Phys. Rev.* C **96** 054303
[39] Nomura K, Rodríguez-Guzmán R, Robledo L M and Garcí-Ramos J E 2021 *Phys. Rev.* C **103** 044311

[40] Spevak V, Auerbach N and Flambaum V V 1997 *Phys. Rev.* C **56** 1357–69
[41] Dobaczewski J and Engel J 2005 *Phys. Rev. Lett.* **94** 232502
[42] Ellis J, Lee J and Pilaftsis A 2011 *J. High Energy Phys.* JHEP11(2011)045
[43] Dobaczewski J, Engel J, Kortelainen M and Becker P 2018 *Phys. Rev. Lett.* **121** 232501
[44] Auerbach N, Flambaum V V and Spevak V 1996 *Phys. Rev. Lett.* **76** 4316–9
[45] Mohanmurthy P, Silwal U, Siwakoti D P and Winger J A 2020 *AIP Conf. Proc.* **2249** 030046
[46] Ahmad I, Gindler J E, Betts R R, Chasman R R and Friedman A M 1982 *Phys. Rev. Lett.* **49** 1758–61
[47] Ahmad I, Chasman R R, Greene J P, Kondev F G and Zhu S 2015 *Phys. Rev.* C **92** 024313
[48] Pritychenko B, Birch M, Singh B and Horoi M 2016 *At. Data Nucl. Data Tables* **107** 1–139